Published in Sensors and Actuators A: Physical 114, issue 1, 80-87, 2004
which should be used for any reference to this work

Development of 1 × 4 MEMS-based optical switch

Z.F. Wang [a,*], W. Cao [b,1], X.C. Shan [a,2], J.F. Xu [b,3], S.P. Lim [b,4], W. Noell [c,5], N.F. de Rooij [c,6]

[a] *Joining Technology Group, Singapore Institute of Manufacturing Technology, 71-Nanyang Drive, Singapore 638075, Singapore*
[b] *National University of Singapore, Singapore 638075, Singapore*
[c] *Institute of Microtechnology, University of Neuchatel, Neuchâtel, Switzerland*

Abstract

In this paper, a novel 1 × 4 optical switch has been developed based on the DRIE vertical mirror technology. Three microactuated vertical silicon mirrors and five tapered/lensed fibers were employed to perform the 1 × 4 switch function. The comb actuators drive the mirrors linearly into the optical path due to the electrostatic force. The tilted mirror with an angle of 22.5° made the layout of the mirrors and optic fibers more compact. Finite element method (FEM) modeling on the linear comb actuator was implemented to verify the design.

Deep reactive ion etching (DRIE) process was employed to fabricate the mirrors, combs and U-grooves on a SOI wafer. A satisfactory yield (up to 70%) was achieved during the microfabrication due to the compactness of the single photomask process. The prototype of the optical switch was packaged and systematically characterized in terms of bonding properties, optical performance including insertion loss, return loss, cross talk, and switch time.

The design and microfabrication has been demonstrated to be successful. The packaging technique can be utilized in the similar category of optical MEMS devices. The optical performance of our switch exhibits the great promise in the application of optical networks.

Keywords: MEMS/MOEMS; Fiber optical switch; Optical packaging; Optical measurement

1. Introduction

To meet the growing demand for high data bandwidth, service providers are building optical networks around the globe using the wavelength-division multiplexing (WDM) technologies with mesh network architecture. Lightpaths between access points in a network are created using fiber links containing many wavelength channels in each fiber, where each channel or port can have a data rate of up to 2.5 or 10 Gb/s [1]. The optical cross-connect (OXC) switches in today's network rely on electronic cores. As port-count and data rates increase, it becomes increasingly difficult for the electronic switch fabrics to meet future demands. It is widely acknowledged that electronic switch fabrics are the bottleneck in tomorrow's communication networks. This bottleneck has stimulated intensive research in developing new all-optical switching technologies to replace the electronic cores [2]. The recent development of free-space optical micro-electromechanical systems (MEMS) technology has enabled the implementations of OXC switching. The superior performance of OXC includes the all-optical mode, low insertion loss, low cross talk, low polarization- and wavelength dependence, higher port-count, and the integration of micro-optics and micro-actuators on the same substrate.

To date, several types of MEMS-based optical switches that have been reported include 1 × 2 switches [3,4], 2 × 2 switches [4–6], 1 × 4 switches [7,8], $N \times N$ 2D or 3D switches ($N = 4, 8, 16, 32, \ldots$) [9–11]. The all-optical 1 × 4 switch is an essential link inside the optical add/drop multiplexers as well as in line systems for network restoration applications [12]. This paper discusses the design, fab-

* Corresponding author. Tel.: +65-67938596; fax: +65-67922779.
E-mail addresses: zfwang@simtech.a-star.edu.sg (Z.F. Wang), wenqing@lanl.gov (W. Cao), xcshan@simtech.a-star.edu.sg (X.C. Shan), ftjx@uaf.edu (J.F. Xu), mpelimsp@nus.edu.sg (S.P. Lim), wilfried.noell@unine.ch (W. Noell), nico.derooij@unine.ch (N.F. de Rooij).
[1] Tel.: +1-505-6651332.
[2] Tel.: +65-67938560; fax: +65-67922779.
[3] Tel.: +1-907-474-5022.
[4] Tel.: +65-69742235.
[5] Tel.: +41-32-7205548; fax: +41-32-7205711.
[6] Tel.: +41-32-7205303; fax: +41-32-7205711.

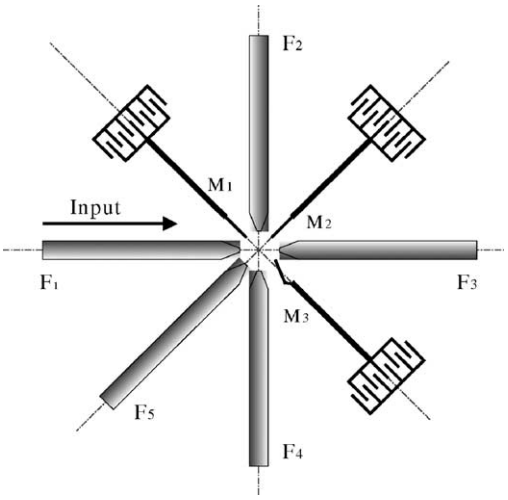

Fig. 1. Top view of the 1 × 4 switch scheme.

rication, packaging, and characterizations done during the development of 1 × 4 switch.

2. Design

2.1. Operation

The working principle of the 1 × 4 switch is shown in Fig. 1. Three microactuated vertical silicon mirrors, M_1–M_3, and five tapered/lensed fibers, F_1–F_5, are employed to perform the 1 × 4 switch function. When a working voltage is applied to any one of the comb actuators the associated mirror, M_1, M_2, or M_3, will be driven linearly into the optical path due to the electrostatic force. Thus, the input light is reflected by the mirror to the fiber F_4, F_2, or F_5, respectively. Without a voltage applied to any comb structure, the mirrors will be pulled back by an attached spring. The input light is reflected to the fiber F_3. In order to reflect the input light to the fiber F_5, the mirror M_3 is tilted with an angle of 22.5° as shown in Fig. 1.

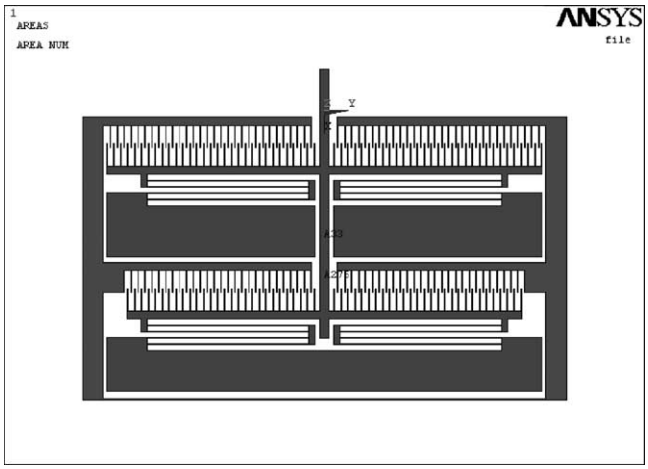

Fig. 2. Design diagram of a comb unit.

2.2. Simulation

The three mirrors in this 1 × 4 switch are driven by the electrostatic forces of three identical comb units, respectively. In order to analyze the actuation performance and stress distribution, finite element method (FEM) modeling on the linear comb actuator was performed using ANSYS v6.0. Quadrilateral elements were used for area meshing. Fig. 2 shows the comb unit which consists of staked combs, springs, and a beam connected with a mirror. Fig. 3 shows the deformation of the comb unit under a voltage of 60 V.

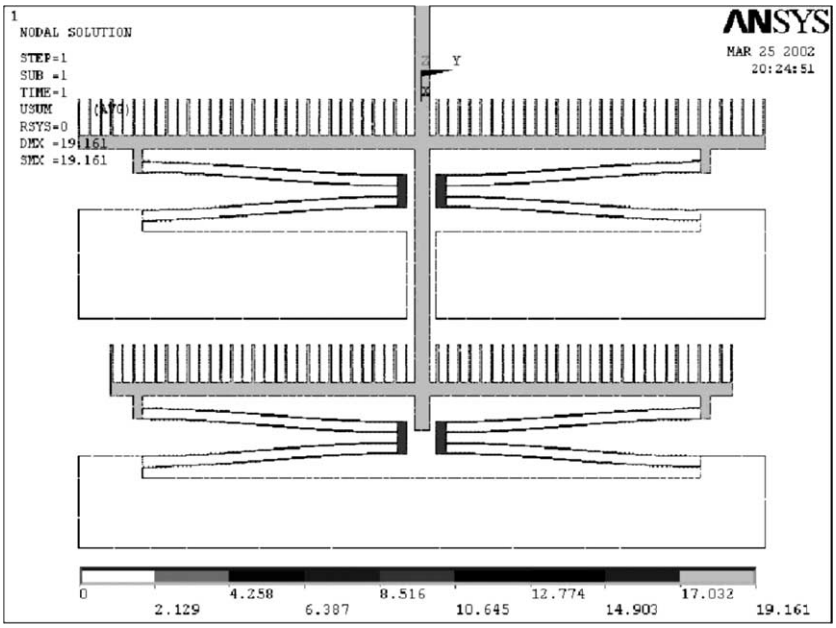

Fig. 3. Deformation of the comb under a voltage.

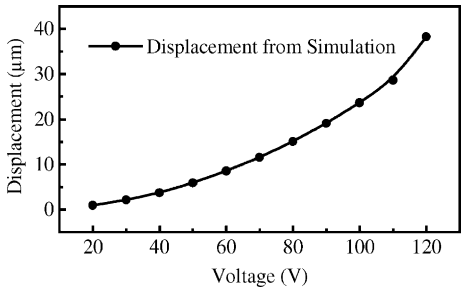

Fig. 4. Displacement of the beam vs. the applied voltage.

The relationship between the displacement of the beam and the voltage is depicted in Fig. 4. This result indicates that a moving range of 30 μm can be obtained under an acceptably low operating voltage of 83 V. The vector plot for principal stresses for the comb actuator model indicates the stress concentration as shown in Fig. 5. It reveals that the principal stress is mainly concentrated within the spring beams. The spring connection beam has a large deformation due to the electrostatic forces. The Von Mises stresses are plotted using the path plot. The value is about 0.5% of the material failure stress [13], which indicates that the single crystal silicon can be used in this application.

3. Fabrication

A silicon-on-insulator (SOI) wafer was used to fabricate the optical switch. The thicknesses of top silicon layer and buried oxide layer are 75 and 2 μm, respectively. The lateral schematic view of the switch structure is shown in Fig. 6. All the mechanical parts, including mirrors, fiber grooves, actuators and suspended springs, were fabricated from the top silicon layer using the deep reactive ion etching (DRIE) process. This monolithic integration process is beneficial to the fiber alignment that considerably determines the light beam

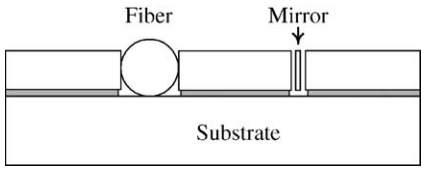

Fig. 6. Lateral schematic view of the switch structure.

coupling efficiency. In order to release the mechanical parts, the buried oxide layer was then partially etched in a buffered aqueous hydrofluoric acid solution. To increase the optical reflectivity, the vertical mirrors were coated with gold using the electron-beam evaporation after the mechanical structures had been released. During the electron-beam evaporation, the devices were oriented appropriately for coating the vertical mirror surfaces. After dicing, the die size is 3.6 mm × 3.6 mm.

Prior to packaging, pre-characterizations were performed. Fig. 7a and b show the SEM images of a comb actuator and the optical path comprising mirrors and grooves. The height and thickness of the micromirrors are 75 and 1.4 μm, respectively. The surface roughness of micromirrors is one of the most important factors for reflectivity. It was measured by AFM. A mirror was transferred and attached to a ceramic substrate for scanning. Fig. 8a and b show an AFM image of micromirror surface and its roughness analysis, respectively. As depicted in Fig. 8b, the average roughness in an area of 10 μm × 10 μm is 2.453 nm. This small roughness value is beneficial to insertion loss in cross state. Fig. 9 shows the displacement of a mirror versus the voltage applied to the linked comb. As a reference, the simulation result in doted line is also shown in Fig. 9. Over-etch can produce structures that are too deep or feature widening if stop layers are used. This could be one of the explanations for the difference between the results of simulation and actual test. Another possible reason could be due to the modulus of elasticity error between the simulation setting and the actual value.

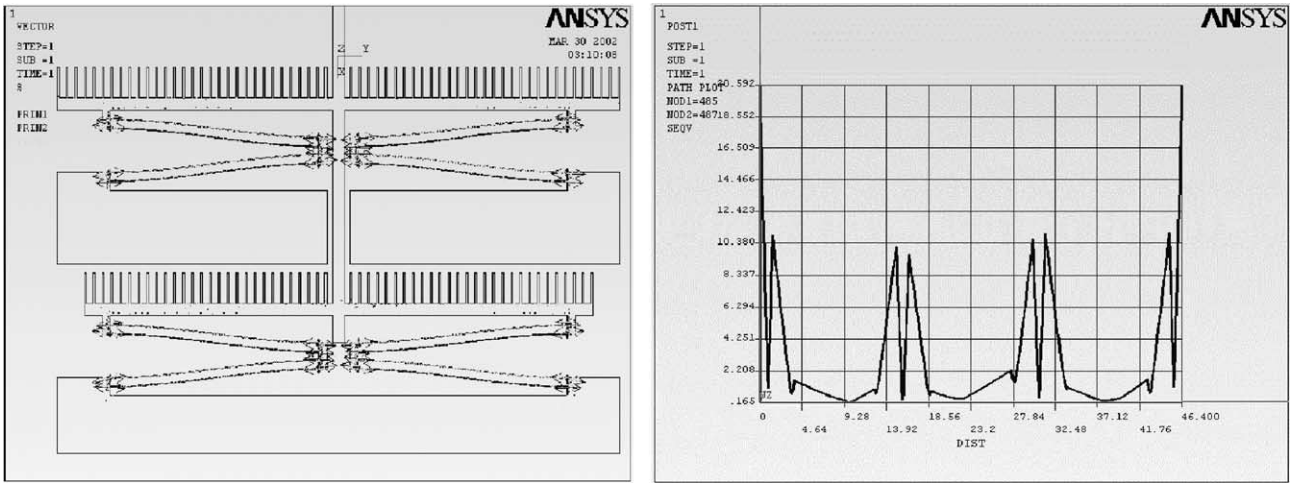

Fig. 5. Von Mises stress distribution on the spring of a comb actuator.

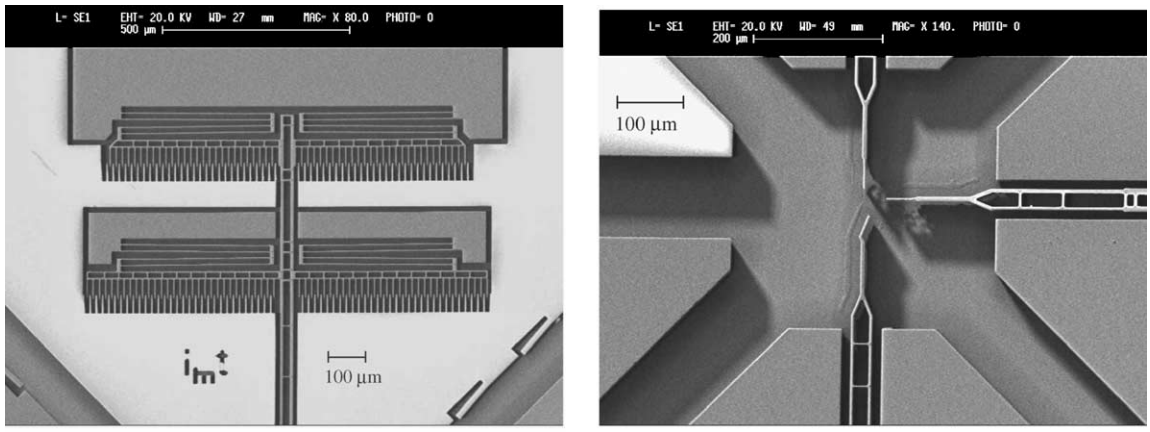

(a) (b)

Fig. 7. SEM images: (a) comb structure, and (b) optical path.

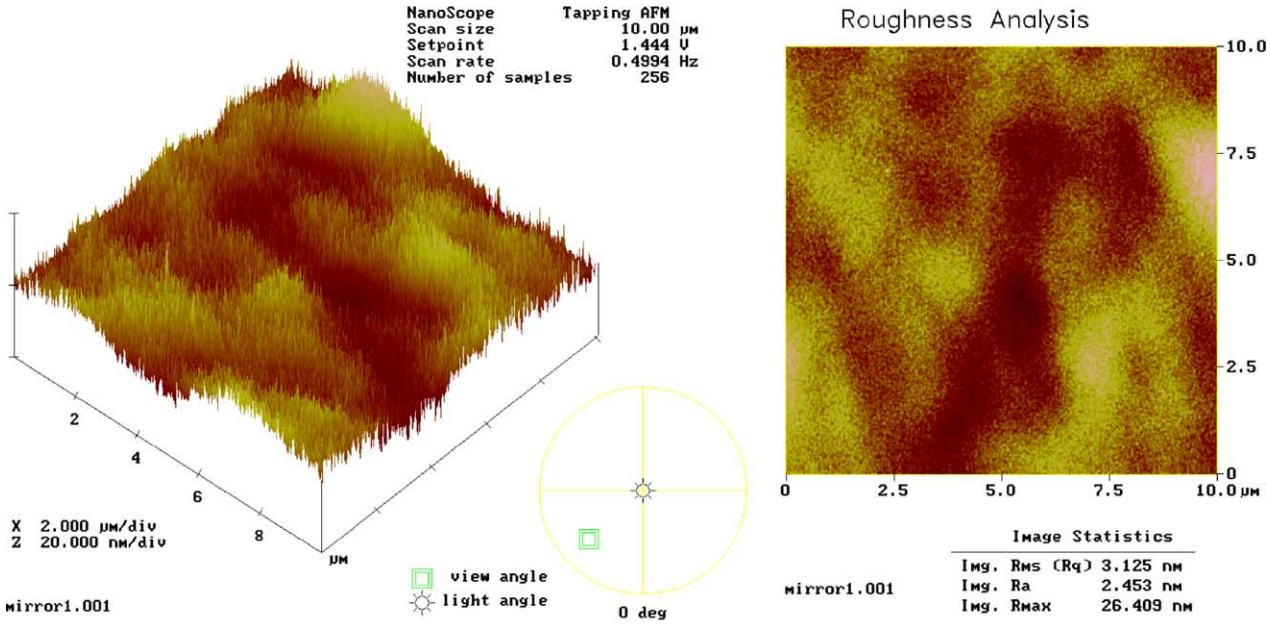

(a) (b)

Fig. 8. (a) AFM image of micromirror surface, and (b) roughness analysis.

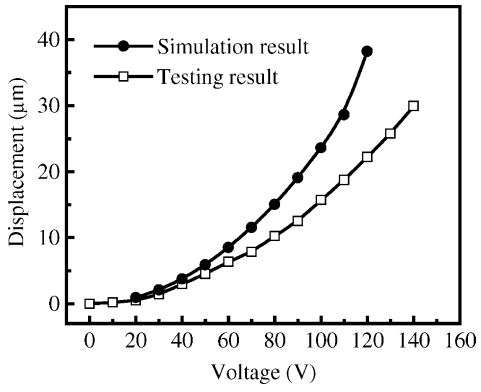

Fig. 9. Displacement of a mirror vs. the voltage applied.

4. Packaging

4.1. Packaging scheme

The purpose of packaging this fiber optic MEMS switch is to connect and protect: establish the optical coupling and optical paths by pigtailing the chip with fibers and connectors, provide electrical connection for control, and protect the structure from contamination, mechanical shock and humidity.

Fig. 10 shows the packaging scheme of the 1×4 fiber optical switch prototype. After dicing the fabricated wafer, the MEMS chip was mounted on a customized ceramic substrate on which the wire bonding pads had been deposited.

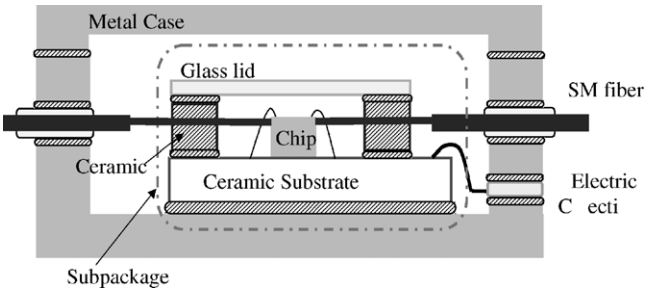

Fig. 10. Packaging scheme of prototype.

The ceramic substrate, a ceramic frame, and a glass lid were used to construct a subpackage indicated in Fig. 10. The packaging ends up with the metal case pigtailed with five optical fibers and FC/PC connectors, and a five-pin electrical connector for plug-in.

4.2. Optical fiber assembly, alignment, and bonding

The eventual optical performance largely depends on not only the fabricated chip but also the tip shape of the optical fiber, assembly and bonding of the fiber. Therefore, the lensed/tapered fibers and adhesives from different manufacturers should be evaluated carefully. The key optical performance parameters of our customized lensed fibers in terms of working distance, mode field diameter, and coupling efficiency are 300 and 8 μm, and 85%, respectively. Fiber assembly and bonding in the silicon groove is another critical issue for the packaging. The precisely designed and fabricated U-groove, incorporating a suspended spring that serves as a stopper, effectively positions and secures the fiber during assembly. Fig. 11 shows a cross-section of a fiber bonded in a U-groove. With proper wetting on a clean surface, the epoxy was well dispensed on the fiber surface around the U-groove. It also reveals that the fiber stands precisely on the bottom of the U-groove. The measurement results of the bonding strength between the fiber and U-groove will be described in Section 5.

Fig. 12 shows the final package of a 1×4 optical switch prototype with a dimension of 35 mm × 25 mm × 10 mm ex-

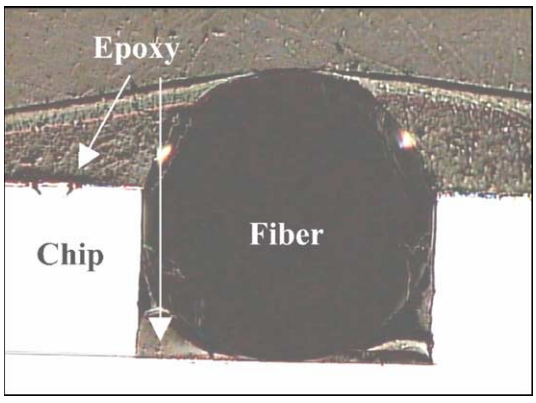

Fig. 11. Cross-section of a fiber bonding to a U-groove.

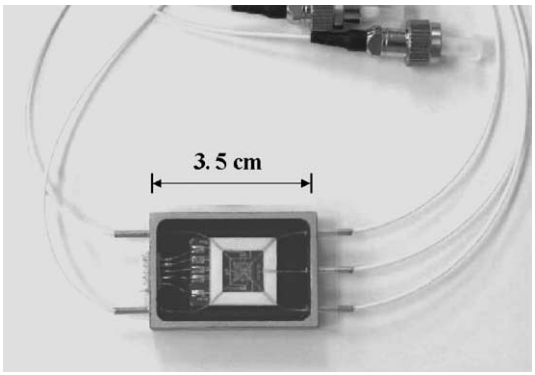

Fig. 12. Prototype of a packaged 1×4 optical switch.

cluding the case cover. Ultimately, the metal case, fiber, and electrical connector were encapsulated to give a hermetic seal.

5. Characterization results

The bonding properties and optical performances of the packaged switch were characterized.

5.1. Bonding properties

A bare fiber was bonded in an U-groove using epoxy for a retention test. In order to determine the bonding strength of a fiber in a U-groove, a pull test was carried out. The force was applied along the direction of the bonded fiber. When the applied force increased beyond 4.5 N, the optical fibers of all samples broke without any debonding of the adhesive. After the testing, all the bonding points are intact. Meanwhile, optical switches are to be subjected to straight pull test for the fibers. This test is intended to verify mechanical robustness and also exposes the switches to conditions that may be experienced during packaging, handling, or installation. In our packaging, the fiber was bonded to the metal tube using epoxy. Following the test procedure of GR-1073-CORE, the generic test requirements for singlemode fiber optic switches [14], 1.0 kg (9.8 N) load was applied to the loose-buffered fiber for 5 s and repeated three consecutive times. All five samples were intact. To further investigate the bonding strength, the debonding forces were characterized to be between 20 and 25 N. These values are more than two times the requirement of GR-1073-CORE.

Gas leakage of the subpackage was characterized to investigate the hermetical encapsulation property. A sample was put into a customized bombing chamber for helium test. Then the chamber was pumped to 10^{-2} mbar, followed by filling with helium gas. Once the He pressure got to 3 bar, the atmosphere was maintained for 2 h. Eventually the subpackage was moved out from the chamber and shifted into He leak detector, Varian^{TM} 959, with a minimum detectable leakage of 10^{-10} std cc/s. The result indicated that the leakage rate of the hermetically sealed subpackage was lower

than 10^{-7} std cc/s. From the view of avoiding moisture and other corrosive ingredients, the leakage of 1×10^{-7} std cc/s would prove reliable for the packaging of the microswitch [15].

5.2. Optical performance: insertion loss, return loss, cross talk, switch time

As the essential parameters of optical switch, insertion loss, return loss, and switch time were characterized following the procedures and requirements of international standards [14,16,17]. The test equipments included DFB source module and power detector module in Newport™ 8800, detector module in ORINON™ fiber auto-alignment system, Newport™ F-CPL-S12155 coupler (1×2 type), and the fiber adaptors. The center operating wavelength is 1550 nm.

5.2.1. Insertion loss

The insertion loss is the fraction of power transferred from input port i to output port j expressed in units of db [14]. Insertion loss depends on the input–output connection (i, j), wavelength, and also depend on switch state. The insertion loss of connection (i, j) at wavelength λ and a given switch state is designated $\mathrm{IL}_{ij}(\lambda)$ and is defined by the following equation:

$$\mathrm{IL}_{ij}(\lambda) = -10 \log_{10} \frac{P_j(\lambda)}{P_i(\lambda)} \tag{1}$$

where, $P_i(\lambda)$ is the optical power launched into port i at center wavelength λ and $P_j(\lambda)$ the on-state optical power measured at port j at center wavelength λ and a given switch state.

The insertion losses in two states, bar state and cross state, were characterized. All the readings were taken repeatedly in order to reflect the errors caused by the connection difference.

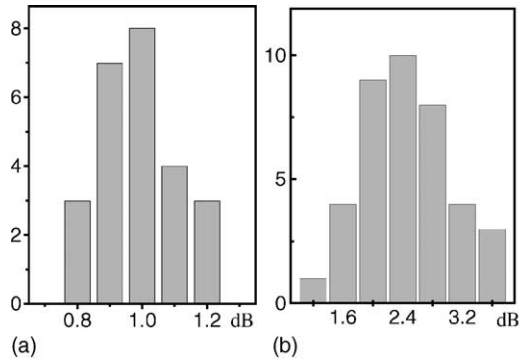

Fig. 13. Insertion losses and their distributions for: (a) bar state and (b) cross state.

The characterization results and their distributions depicted in Fig. 13 exhibit considerable repeatability.

5.2.2. Return loss

Return loss measures the cumulative effect of all backscatter and parasitic reflections from within the device. Return loss depends on the port, wavelength, and may depend on the switch state [14].

$$\mathrm{RL}_i(\lambda) = -10 \log_{10} \frac{P_{i\,(\mathrm{back})}(\lambda)}{P_{i\,(\mathrm{in})}(\lambda)} \tag{2}$$

where $P_{i\,(\mathrm{in})}(\lambda)$ is the optical power launched into port i, and $P_{i\,(\mathrm{back})}(\lambda)$ the off-state optical power returning to port i at center wavelength λ.

Following the measurement procedure in TIA/EIA Standard [17], the characterization scheme was set up as Fig. 14a and b. The power levels P_0 at the detector at coupler port 1 and P_1 at the detector at coupler port 3 were measured in Fig. 14a. In order to reduce the reflection from detector 1, the fiber between port 1 and detector 1 was wrapped

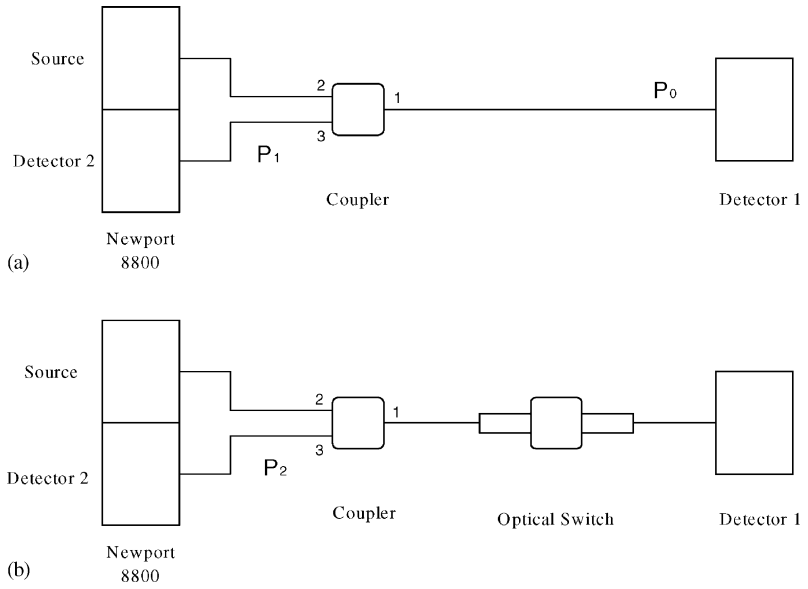

Fig. 14. Measurement setup of return loss.

in mandrel with a diameter of 15 mm when the readings of P_1 were taken. Subsequently, the detector was disconnected from coupler P_1. Connect the switch to coupler port 1, and the detector as shown in Fig. 14b. The mandrel wrap of 15 mm of the optical fiber between the switch and detector 1 was applied to reduce the reflection when the readings of P_2 were taken. The calculation of return loss is formulated [17] as

$$\mathrm{RL} = -10\log_{10}\left[\frac{c - P_1}{P_0}\right] - \mathrm{IL} \tag{3}$$

where, RL is the return loss; IL the coupler insertion loss; P_0, P_1 and P_3 are the readings of power described above.

Following above method, the return loss of optical switch was characterized. The readings were taken repeatedly to minimize the errors caused by the connection difference. The characterization results and their distribution are depicted in Fig. 15. The results include bar- and cross states. Therefore, the distribution broadens slightly.

5.2.3. Cross talk

The cross talk is the fraction of power transferred from input port *i* to an unintended output port *j* expressed in unit of db. Cross talk depends on the input and out put ports (*i* and *j*), wavelength, and may also depend on switch state. The cross talk, $\mathrm{XT}_{ij}(\lambda)$, from input port *i* to output port *j* at wavelength λ and for a given switch state is defined by the following equation [14]:

$$\mathrm{XT}_{ij}(\lambda) = -10\log_{10}\frac{P_j(\lambda)}{P_i(\lambda)} \tag{4}$$

where, $P_i(\lambda)$ is the optical power launched into port *i* at center wavelength λ and $P_j(\lambda)$ the off-state (i.e. when connection (*i*, *j*) is in the off-state) optical power measured at port *j* at center wavelength λ and a given switch state.

The cross talk of our optical switch was characterized. The results were over 35 db in the cross state and over 60 db in the bar state.

5.2.4. Switch time

The connection switch-on time, t_{ON}, is a measure of how fast a connection can be established. It is measured from the initial application of the control signal to the time it takes the output power to increase to 90% of the on-state steady state optical power level, with no subsequent ringing greater than 10%. The switch-on time includes both the control signal transients and the optical signal transients. Similarly, The connection switch-off time, t_{Off}, is a measure of how fast a connection can be broken. It is measured from the initial removal of the control signal to the time it takes the output power to fall to 10% of the on-state steady state optical power level, with no subsequent ringing greater than 10% [14].

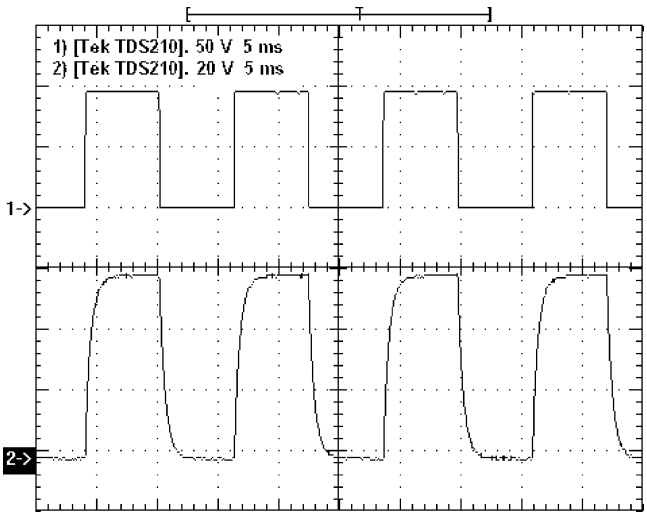

Fig. 16. Control and optical signal waveforms of 1×4 optical switch.

Fig. 16 shows four working cycles of 1×4 optical switch at a operating voltage of 90 V. The above curve labeled as 1 in Fig. 16 is control waveform and the below curve labeled as 2 is reflected optical signal. The optical switch can work steadily. Both the switch-on and switch-off times are 0.8 ms. This switching time of 0.8 ms is only 1/12 of the generic switching time criteria [14].

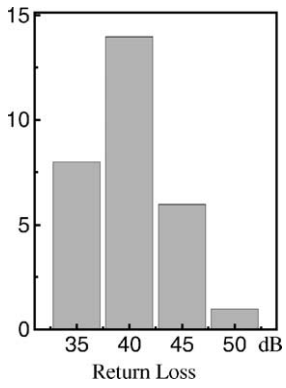

Fig. 15. Return losses and their distribution.

6. Conclusions

We have designed and fabricated a novel 1×4 optical switch based on SOI wafer and DRIE process. The tilted mirror with an angle of 22.5° made the layout of the mirrors and optic fibers more compact. Only one photomask is needed to fabricated the micromirrors, comb structures and connected springs, U-groove, and a suspended spring (stopper). A satisfactory yield of 70% was achieved during the microfabrication. The precision U-groove with an integrated stopper and our customized lensed fibers is a novel approach for easy assembly and alignment of optical fibers. The optical switch prototype was packaged and systematically characterized in terms of bonding properties, optical performance including insertion loss, return loss, cross talk, and switch time. Even though the comb and associated spring structure could be further optimized, the 1×4 optical switch is ready for immediate applications in optical networks today.

Acknowledgements

This project was funded by Agency for Science, Technology and Research (A*STAR), Singapore.

References

[1] P.B. Chu, S.S. Lee, S. Park, MEMS: the path to large optical cross-connnects, IEEE Commun. Mag. 40 (3) (2002) 80–87.
[2] T. Yeow, K.L.E. Law, A. Goldenberg, MEMS optical switches, IEEE Commun. Mag. 39 (11) (2001) 158–163.
[3] S.S. Lee, L.Y. Lin, M.C. Wu, Surface micromachined free space fiber-optic switches, Electr. Lett. 31 (17) (1995) 1481–1482.
[4] M.M. Koh, W. Menz, Micro optical switching by electrostatic linear actuators with large displacements, in: Proceedings of the Seventh International Conference on Solid-State Sensors and Actuators, Yokohama, Japan, 1993, pp. 120–123.
[5] A. Müller, J. Göttert, J. Mohr, LIGA microstructures on top of micromachined silicon wafers used to fabricated a micro-optical switch, J. Micromech. Microeng. 3 (1993) 158–160.
[6] C. Marxer, N.F.D. Rooij, Micro-opto-mechanical 2 × 2 switch for single-mode fiber based on plasma-etched silicon mirror and electrostatic actuation, IEEE J. Lightwave Technol. 17 (1999) 2–6.
[7] M. Hoffmann, E. Voges, Bulk silicon micromachining for MEMS in optical communication systems, J. Micromech. Microeng. 12 (2002) 349–360.
[8] M. Hoffmann, P. Kopka, D. Nüsse, E. Voges, Fibre-optical MEMS switches based on bulk silicon micromachining, Microsyst. Technol. 9 (5) (2003) 299–303.
[9] D.J. Bishop, C.R. Giles, G.P. Austin, The Lucent LambdaRouter: MEMS technology of the future here today, IEEE Commun. Mag. 40 (3) (2002) 75–79.
[10] P.B. Chu, S.S. Lee, S. Park, MEMS: the path to large optical cross-connects, IEEE Commun. Mag. 40 (3) (2002) 80–87.
[11] P.D. Dobbelaere, K. Falta, L. Fan, S. Gloeckner, S. Patra, Digital MEMS for optical switching, IEEE Commun. Mag. 40 (3) (2002) 88–95.
[12] A. Neukermans, R. Ramaswami, MEMS technology for optical networking applications, IEEE Commun. Mag. 39 (1) (2001) 62–69.
[13] C. Wilson, P. Berk, Fracture testing of bulk silicon micro-cantilever beams subjected to a side load, J. Microelectromech. Syst. 5 (1996) 142–150.
[14] Telcordia Technologies GR-1073-CORE: Generic Requirements for Singlemode Fiber Optic Switches, January 2001.
[15] Y.F. Jin, Z.F. Wang, Z.P. Wang, A study on hermetic packaging for micro-optical switch, in: Proceedings of IEEE Fourth Electronics Packaging Technology Conference, Singapore, 2002, pp. 96–100.
[16] TIA/EIA Standard: Interconnection Device Insertion Loss Test, TIA/EIA-455-34A, November 1995.
[17] TIA/EIA Standard: Determination of Component Reflectance or Link/System Return Loss Using a Loss Test Set, TIA/EIA-455-107A, March 1999.

Biographies

Zhenfeng Wang was born in Shanghai, China. He received his BEng and PhD in electrical engineering (1996) from Tsinghua University, Beijing, China. From 1996 to 1998, he worked at Nanyang Technological University (NTU), Singapore as a postdoctoral fellow. In 1996, he joined Singapore Institute of Manufacturing Technology (SIMTech). He is currently a research scientist at SIMTech involved in microsystem integration and micromachining process development. During the last 5 years, he has been collaborating with scientists from the Institute of Microtechnology of the University of Neuchâtel, Switzerland in the field of MEMS device development.

Wenqing Cao received the BSc and MSc degrees from Xidian University, China, in 1986 and 1992, respectively, and the PhD from Nanyang Technological University, Singapore, in 2002. He is currently a postdoc at Los Alamos National Laboratory, USA. His research interests are in fiber-optic evanescent chemical sensors, semiconductor oxide-based gas sensors, MEMS/MOEMS and their packaging.

Xue Chuan Shan received his PhD degree from Tohoku University in 1992. From 1992 to 1998, he worked in Olympus Optical Co. Ltd. as a senior research engineer. He then joined in Singapore Institute of Manufacturing Technology (former Gintic) as a research scientist. From October 2001 to December 2002, he worked in the Advanced Industry Science and Technology (AIST), Japan as a visiting research scientist. His research interests include AFM-related techniques, design, fabrication and packaging of microsystems, and microhot embossing.

Jianfeng Xu received his MSc of Singapore-MIT Alliance in 2002. His research interests include coupled MEMS modeling, simulate and analysis the mechanical property of the miniature structures. He is currently studying for PhD in University of California at San Diego.

Wilfried Noell received the PhD degree in physics from the University of ULM, Germany, in 1998. Since 1998, he is with the Institute of Microtechnology (IMT), University of Neuchâtel, Switzerland. After working for more than 2 years on tools for nanoscience he became responsible for the group's activities on optical microsystems in the beginning of 2001. The PhD work was pursued externally at the Institute for Microtechnology Mainz (IMM), Germany, on the development of a microfabricated optical near-field sensor. He finished his physics studies with a diploma degree at the Technical University of Darmstadt (TUD), Germany, in 1994. His diploma thesis was a joined work between the applied optics group of the physics department of TUD and the research and technology center (FTZ) of the Deutsche Telekom on integrated optical waveguides based on InP.

Nicolaas F. de Rooij received a M.Sc degree in physical chemistry from the State University of Utrecht, The Netherlands, in 1975, and a PhD degree from Twente University of Technology, The Netherlands, in 1978. From 1978 to 1982, he worked at the Research and Development Department of Cordis Europa NV, The Netherlands. In 1982, he joined the Institute of Microtechnology of the University of Neuchâtel, Switzerland (IMT UNI-NE), as professor and head of the Sensors, Actuators and Microsystems Laboratory. Since October 1990 till October 1996 and again from October 2002, he is acting as director of the IMT UNI-NE. He lectured at the Swiss Federal Institute of Technology, Zurich (ETHZ), and since 1989, he has been a part-time professor at the Swiss Federal Institute of Technology, Lausanne (EPFL). His research activities include microfabricated sensors, actuators, and microsystems. He was a member of the steering committee of the International Conference on Solid-State Sensors and Actuators and of Eurosensors. He acted as European Program Chairman of Transducers '87 and General Chairman of Transducers '89. He is a member of the editorial boards for the journals *Sensors and Actuators, Sensors and Materials*and *the IEEE Journal of Microelectromechanical Systems*. Dr de Rooij is an IEEE fellow.